Geophysical Research Letters

RESEARCH LETTER
10.1029/2024GL112582

Impact of Climate Change on the Dynamics of the Southern Senegal Upwelling Center

S. Ndoye[1,2,3], V. Echevin[2], J. Mignot[2], and X. Capet[2]

[1]Université Amadou Mahtar MBOW, UFR des Sciences et Technologies Avancés (STA), Dakar, Senegal, [2]Laboratoire d'Océanographie et du Climat: Experimentations et Approches Numériques (LOCEAN-IPSL), Sorbonne Université, CNRS, IRD, MNHN, Paris, France, [3]Laboratoire de Physique de l'Atmosphère et de l'Ocean Siméon Fongang, ESP/UCAD, Dakar, Senegal

Key Points:

- A CMIP5 high CO2 emission climate change (CC) projection is downscaled in the West African coastal ocean using a regional circulation model
- The 10% reduction of upwelling favorable wind found in CMIP5 for the end of the century weakens coastal upwelling by 15%
- Adding CC induced temperature and salinity perturbations leads to a stronger weakening of coastal upwelling by 25%

Supporting Information:

Supporting Information may be found in the online version of this article.

Correspondence to:

S. Ndoye,
siny.ndoye@uam.edu.sn

Citation:

Ndoye, S., Echevin, V., Mignot, J., & Capet, X. (2025). Impact of climate change on the dynamics of the southern Senegal upwelling center. *Geophysical Research Letters*, *52*, e2024GL112582. https://doi.org/10.1029/2024GL112582

Received 20 SEP 2024
Accepted 9 JAN 2025

Abstract The Canary current upwelling System (CCS) is one the most productive marine ecosystems. CMIP5 simulations under the RCP8.5 scenario for the end of the 21st century project a modest upwelling-favorable wind decrease over the CCS southern outpost, that is, the southern senegalese upwelling center (SSUC). We explore the coastal-scale physical manifestations of climate change in the SSUC through dynamical downscaling of projected changes from nine CMIP5 models selected for their realistic representation of present-day thermohaline structure. We find that coastal upwelling reduction due to wind changes is projected to be aggravated by geostrophic/pressure adjustments related, in large part, to changes in upper ocean stratification. The reduction could reach 25% of present-day upwelling rates. The intensity of the poleward boundary current offshore of the SSUC is projected to decrease. Together with upper ocean warming this opens vast possibilities of ecological evolutions with large impact on neighboring societies.

Plain Language Summary The impact of climate change in the coastal ocean off West Africa is studied numerically using a regional ocean model resolving fine-scale dynamics. Under normal conditions, the coastal wind blows southward during the cold season (January–May) which generates upwelling of deep, cold and nutrient-rich waters south of the Cap Vert peninsula (15°N). Abundant planktonic species grow within the cold water plume spreading southward. Using winds, temperature and salinity projected by climate models for a high CO2 emission world, we force the regional model and find a substantial reduction of the upwelling (by up to 25%) and a warming of the upper layer of the ocean (0–100 m) by 3-4°C. This may have drastic impacts on West African coastal ecosystems.

1. Introduction

There is growing evidence that subtropical highs will shift poleward as a consequence of climate change (CC) and this may already be underway in the case of the Azores high pressure (Bograd et al., 2023; Rykaczewski et al., 2015; Sylla et al., 2019; Wang & Jordi, 2011).

At the southern end of the Canary Current Upwelling System (CCS) sits the Southern Senegal Upwelling Center (SSUC). The SSUC upwelling pattern is very robust in time (Capet et al., 2017; Ndoye et al., 2017), with a localization of upward vertical velocities south of Cape Verde (15°N) (Ndoye et al., 2017) and an upwelling plume predominantly oriented alongshore (Demarcq & Faure, 2000; Ndoye et al., 2014). The coastal domain benefiting from enrichment by the SSUC plume can span up to 3 degrees of latitude over the coastal shores of Senegal, Gambia (13.2-13.6°N), and, to a lesser extent, Guinea Bissau (12°N). Upwelling in the SSUC is strongly modulated on seasonal time scales with a core upwelling season in January–May and a near halt in July–October when the ITCZ is located over the area (Fall et al., 2006). The SSUC circulation is bordered by the poleward subsurface West African boundary current (WABC) (Barton, 1998; Hughes & Barton, 1974; Kounta et al., 2018; Mittelstaedt, 1991) carrying the source water masses of the SSUC, and intensified by cyclonic wind stress curl driving a poleward Sverdrupian flow (Kounta et al., 2018). WABC variability exerts a major influence over the productivity and ventilation of the Senegalese (e.g., (Tall et al., 2021)) and Mauritanian continental shelves (Klenz et al., 2018). The southern CCS is also among the least studied of coastal oceans (Capson et al., 2021). The future evolution of its main features (e.g., coastal upwelling, WABC, biogeochemical conditions) are unknown. Here we thrive to study the physical consequences of CC, focusing on the SSUC.

Because of their coarse spatial resolution (∼50–200 km), global climate models (GCMs) employed in the Coupled Model Intercomparison Project (CMIP) phases are generally not suited to address coastal ocean changes. Our approach follows the classical dynamical downscaling strategy whereby GCMs provide oceanic initial and boundary conditions to fine-resolution (∼2–10 km) regional ocean models (Bograd et al., 2023; Echevin et al., 2012; Machu et al., 2015; Oerder et al., 2015).

Precisely, CC seasonal perturbations are computed using a suited subset of CMIP5 model outputs. Choosing a multi-model ensemble reduces the potential biases introduced by the choice of a single model (Lee et al., 2013; Vázquez et al., 2023). CC perturbations are then added to the regional ocean model present-state forcing fields (whose interannual variability is thus applied into the future, i.e., we assume it remains unchanged during late 21st century). Sensitivity simulations using various CC density perturbations (no change, horizontally constant or horizontally variable change) allow us to isolate the roles of different forcings. Most notably, we find substantial reductions in SSUC upwelling intensity (∼25%) in 2080–2100 attributed in roughly equal proportion to wind stress decrease and upper ocean stratification increase. Methodology and results are respectively presented in Sections 2 and 3. A discussion and concluding remarks are offered in Section 4.

2. Materials and Methods

To investigate the changes in SSUC circulation and upwelling, the regional-scale sensitivity experiments are carried out with forcings (air-sea fluxes, lateral ocean boundary conditions, and initial conditions) perturbed by CC signals derived from CMIP5. Results are compared with a reference simulation for the historical period. The domain of interest being of the size of a (few) GCM grid boxes, our downscaling strategy will leave a large buffer zone between where CMIP5 oceanic perturbations are imposed and the senegalese coastal ocean.

2.1. Regional Model Setup

The Regional Ocean Modeling System (ROMS) (Shchepetkin & McWilliams, 2005) with AGRIF 2-way nesting (Debreu et al., 2012) is used. ROMS solves the hydrostatic primitive equations using terrain-following curvilinear coordinates. The model setup is based on the configuration of Ndoye et al. (2017) utilized to investigate the SSUC present-day dynamics and also used in Chabert et al. (2023). The parent grid extends from 6° to 35°N and from to 6° to 32°W, that is, it covers most of the CCS, with a horizontal resolution of $\Delta x \sim 10$ km. A child grid the Senegalese coastal ocean (from 12°N to 18°N and from to 20°W to 15°W) with a resolution of $\Delta x \sim 2$ km, which is sufficient to represent frontal processes in the SSUC (Ndoye et al., 2017).

2.2. Reference Simulation

The "present-day" reference simulation (S_{Ref}) was presented and analyzed in Ndoye et al. (2017). It adequately captures key observed fine-scale (20–100 km) SST features, including the predominance of upwelling within 25–50 km south of Dakar. This implies that the circulation is also realistically simulated, as subsequently confirmed by a comparison with in situ data (Chabert et al., 2023).

Its main characteristics are recalled here: climatological surface heat/freshwater fluxes and daily QuikSCAT wind stress for the period 1999−2008 were used; heat and freshwater forcings combine ICOADS (Worley et al., 2005) and TropFLUX (Praveen Kumar et al., 2013) data with a restoring term toward observed SST and SSS (Barnier et al., 1995, see Text S1 in Supporting Information S1). Lateral ocean open boundary conditions are taken from a climatology (1999–2008) of the Simple Ocean Data Assimilation (SODA) reanalysis (Carton & Giese, 2008). The interannual variability present in this simulation only arises from the wind stress forcing variability.

2.3. Definition of the Regional Climate Change Perturbations

Because CMIP simulations tend to have large biases relative to state-of-the-art reanalyzes (e.g., Lellouche et al., 2018), they will be used to define late 21st century perturbation fields (hereafter CC perturbations) for the ocean initial/lateral conditions and surface forcings. CC perturbations are computed as seasonally varying differences between the CMIP5 simulations under the historical scenario (period 1985–2005) and the Representative Concentration Pathway (RCP8.5) so-called worst-case scenario (period 2080–2100), and then added to present-day forcings. This approach is classically referred to as the Seasonally Varying Delta Method (Pozo Buil et al., 2023).

Upper ocean stratification can be locally quite unrealistic in CMIP simulations, which may impact the CC perturbations. We assume here that the most realistic CC perturbations will be obtained from the least biased present-day simulations in the region. Although such approach is widely used in the literature (Hall et al., 2019) and alternatives have been proposed recently (Ribes et al., 2022). Such refinements are left for future studies.

We thus select a subset of the CMIP5 ensemble as follows: CMIP5 density profiles are averaged over the Senegalese-Mauritanian region (12°N-20°N 16°W-20°W) for part of the historical period (1985–2005); CMIP5 and WOA spatially averaged profiles (Boyer et al., 2018) are compared over the top 200 m of the ocean; GCMs with a depth-average RMS error exceeding 0.03 kg m^{-3} are discarded. This leaves 9 models (see Table S1 in Supporting Information S1) to compute the ensemble mean CC perturbations from monthly climatologies over 2080–2100 (future period) and 1985–2005 (present period). The performance of all CMIP5 models in representing other key variables such as present-day SST and wind stress patterns associated with upwelling are shown in Sylla et al. (2019). The models are generally able to reproduce the seasonal cycle of upwelling favorable wind fairly well and this is also true for the ones we selected. The realism of modeled SST seasonal cycle is not nearly as good even in terms of coast to open ocean contrast, hence one of the justifications for the sensitivity study to the regional form of thermohaline perturbations that was conducted as part of this work (see below).

Note that a more elaborate downscaling approach would have consisted in running individual downscaling experiments for each of the retained CMIP5 models and subsequently average their response (e.g., Howard et al. (2020) in the California Upwelling System). This would have increased the energy/CO2 emission footprint of the study by a factor 9 while Howard et al. (2020) suggest that nonlinear effects responsible for differences between the two approaches shall be modest for physical variables.

The treatment of wind forcing perturbations without any downscaling is a reasonable first approach given the regional smoothness of present-day trade winds at these low latitudes (see Figure 15 in Ndoye et al. (2014)), and the absence of major local orographic features, in stark contrast with other upwelling sectors (see Winant et al. (1988),Garreaud and Muñoz (2005), and Particola and Chang (2017) for the California, Chile and southern Benguela system respectively). Remotely generated effects are mainly produced by the large-scale wind patterns (Enfield & Allen, 1980) and shall also be adequately captured to first order. Our procedure to exclude CMIP land winds only consists in nearest neighbor extrapolations of ocean wind perturbations toward the coast prior to their interpolation on ROMS model grids and it does not attempt to improve coastal wind drop off (in contrast to what was done in, e.g., Capet et al. (2004)). Note though that: its magnitude is modest, partly a consequence of lack of orography as suggested by Renault et al. (2015); its momentum forcing effect is largely under frictional control over the continental shelf (which excludes the major Sverdrupian consequences found in other upwelling sectors (Capet et al., 2004; Small et al., 2015)).

2.4. Climate Change Regional Simulations

CC can impact regional ocean dynamics through regional wind and thermohaline changes. Precisely, we perform and analyze three CC sensitivity experiments that differ by their CC perturbations. In simulation S_W, we only introduce the wind stress CC perturbation (details on the procedure can be found in Text S1 in Supporting Information S1). In simulation S_{W-S}, we add temperature ($\delta\theta(x,y,z,t)$); herein δ systematically denotes to future minus present differences) and salinity ($\delta S(x,y,z,t)$) CC perturbations to the initial condition and to the lateral boundary conditions of the parent domain. As the resulting θ and S fields are a priori incompatible with present-day heat and freshwater fluxes, the use of CC perturbations for these forcings would in principle be in order. However, analysis reveals extreme inter-model differences for these quantities which makes the use of the multi-model mean questionable (see Figure S1 in Supporting Information S1). To circumvent this issue, the surface fluxes are only perturbed via the SST and SSS fields entering the restoring terms (e.g., $\mathrm{SST} = \mathrm{SST}_{\mathrm{obs}} + \delta\mathrm{SST}_{\mathrm{CMIP5}}$, see Figure S2 and Text S2 in Supporting Information S1). Another difficulty with S_{W-S} arises from the use of CMIP5 low resolution boundary conditions where we expect major inconsistencies between the representations of bathymetry and coastline in ROMS versus CMIP5 GCMs. This presumably induces deficiencies in the horizontally variable CC perturbations for density and thus for the associated geostrophic velocity CC perturbations. To evaluate the consequences of these inconsistencies, we use a third sensitivity experiment S_{W-SC} in which the thermohaline CC perturbations ($\delta\theta(z,t), \delta S(z,t)$) are equal to their horizontal average over the region (12°N-20°N 20°W-16°W). Differences between S_{W-SC} and S_{W-S} allow us to quantify the dynamical effects of the horizontal heterogeneities present in the CMIP5 thermohaline perturbations

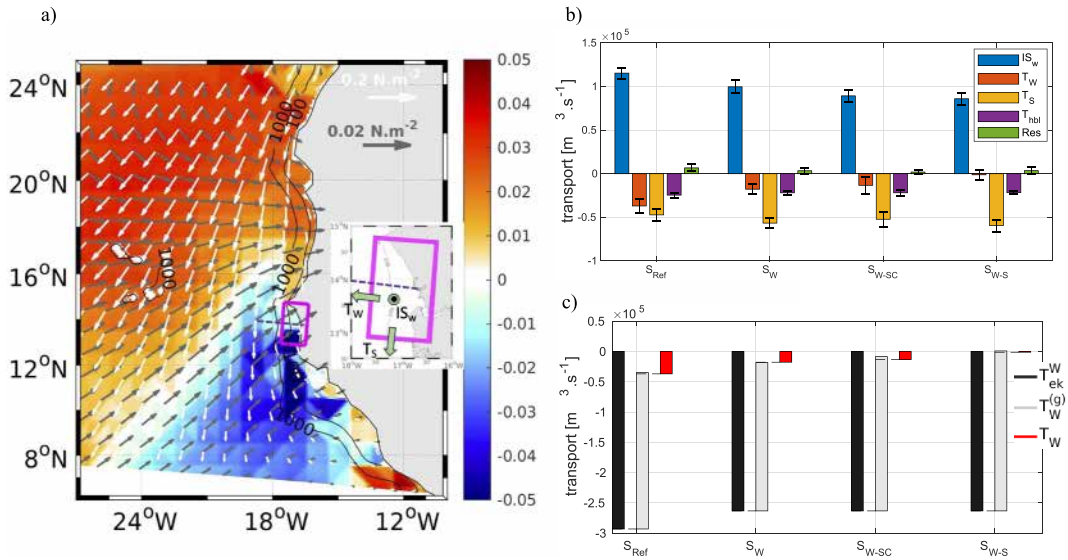

Figure 1. (a) SCOW wind stress climatology (2000–2008; in N m^{-2}; white arrows), CMIP5 wind stress CC perturbation (black arrows) and Ekman pumping change (derived from wind stress curl anomaly; color scale; in m day^{-1}). Values are averaged over the upwelling season (January–May) and anomalies are diagnosed from the CMIP5 selected ensemble (see Table S1 in Supporting Information S1). Note the different wind stress scales marked by horizontal arrows on land. The magenta box defines the SSUC box (~ 17°30'W–16°30'W, 13°N–15°N) used to compute the mass balance. The box is located so that the northern boundary is closed. The box boundaries follow the model grid lines, which are nearly parallel (~ 4.5° deviation) to meridians and parallels. T_W indicates zonal transport through the western boundary of the box, T_S indicates transport through the southern boundary of the box, IS_w indicates vertical transport across the mixed layer base. (b) Mass budget in the reference and climate change simulations. T_{hbl} is the incoming/outgoing transport in the mixing layer and Res is the residual closing the budget. (c) Comparison of zonal transports (in m^3 s^{-1}, see Equation 1) through the western face of the SSUC box: the offshore Ekman transport (T^W_{ek}, negative, black bars), onshore geostrophic transport ($T^{(g)}_W$, positive, gray bars) and the net transport (T_W, red bars) are shown. The residual ϵ_{T_W} which corresponds to the mismatch between the thin dashed horizontal line and the upper limit of the gray bar is negligible.

(on which we have low confidence). Note that thermohaline horizontal heterogeneity can still be internally produced by the regional model in S_{W-SC} (see Figure S6a in Supporting Information S1). Table S2 in Supporting Information S1 summarizes the experimental protocol. Overall, S_W differs from $S_{W-S/SC}$ by its lack of CC perturbations in air-sea heat/salt flux and ocean lateral boundary conditions.

3. Results

3.1. CCS-Scale Patterns of Climate Change

We first present the CMIP5 CC perturbations in relation to the associated present-day fields. 2080–2100 wind anomalies in our study region (Figure 1a, black arrows) are consistent with those found in previous studies (Sylla et al., 2019; He et al., 2017; D'Agostino et al., 2020; Vázquez et al., 2023) with a zonal band (6-20°N) of westerlies induced by the northward shift of the Azores high. Off Senegal, the northeastward wind CC perturbation direction partly opposes upwelling favorable wind. In the coastal sector between 12 and 15°N, the reduction of the upwelling favorable wind in future conditions is the most pronounced (~−10% for the multi-model mean with a decrease reaching ~−20% in a few GCMs; see Figure S3 in Supporting Information S1).

These regional wind changes induce a wind stress curl modulation in the CCS (Figure 1a). Wind stress curl is predominantly positive in the coastal area because land-sea contrasts and the shape of the African continent produce a curvature of the trade winds favorable to cyclonic rotation nearshore and anticyclonic offshore around the North Atlantic subtropical gyre. This has key implications both in terms of vertical and lateral transport, due to Ekman suction and Sverdrup balance/potential vorticity conservation (Kounta et al., 2018). Overall wind stress curl is substantially affected by CC with a nearshore ~10% increase (resp. ~15% decrease) north of 16°N (resp. South of 14°N) owing to the curvature of the wind CC perturbation (Figure 1a). Consequences of this in terms of poleward transport will be shown and discussed below (see Section 3.3).

3.2. Change in SSUC Coastal Upwelling

In simplified (e.g., 2D alongshore invariant) theories of coastal upwelling, the upward flux of subsurface water into the surface layer is determined by the intensity of the wind stress component parallel to shore. The situation is more subtle in the real ocean where alongshore pressure gradients can induce large discrepancies between alongshore wind intensity and actual upwelling circulation as previously shown for the SSUC (Ndoye et al., 2017) and other coastal regions (Colas et al., 2008; Jacox et al., 2018; Marchesiello et al., 2011). In addition, in sectors like the SSUC with abrupt irregularities of the coastline, local upwelling is also modulated by convergence/divergence of the alongshore flow.

To quantify the upwelling changes, we define a control volume encompassing the southern Senegalese shelf (see box in Figure 1a) and vertically limited by the air-sea interface and the base of the mixed layer (ML). Assuming steady state, volume conservation writes:

$$IS_w + T_W + T_S + T_{hbl} = 0 \quad (1)$$

where IS_w is the vertical flux through the ML base of the box (i.e., upwelling rate), T_{hbl} is the horizontal flux into the ML where its base is not flat, and T_W and T_S are respectively the fluxes through the box's western and southern boundaries (see mathematical expressions in Text S3 in Supporting Information S1). In practice, the sum of these terms computed from monthly averaged fields is not strictly zero. We estimate a residual referred to as ϵ.

The quantity of interest is the upwelling rate IS_w which partly determines nutrient enrichment of the system (nutrient concentrations of upwelled waters are also key but cannot be examined in our physical framework). Equation 1 allows us to relate changes in upwelling rate to lateral fluxes in and out of the coastal box. The net cross-shore volume flux at the western boundary T_W can be further decomposed into a geostrophic and Ekman contribution:

$$T_W = T_W^{(g)} + T_W^{(ek)} + \epsilon_{T_W} \quad (2)$$

where $T_W^{(g)}$ and $T_W^{(ek)}$ are respectively the geostrophic and wind-driven Ekman transports (see Text S3 in Supporting Information S1 for their mathematical expression). ϵ_{T_W} subsumes the other non-geostrophic contributions to total transport at the western boundary (advection and bottom friction).

Figure 1b shows all terms in (1) for the reference and CC experiments. It reveals the complexity of the volume conservation balance, with a large southward flow (T_S) out of the box. This confirms the conclusions of Ndoye et al. (2017) that coastal upwelling dynamics in the SSUC strongly deviates from 2D alongshore invariant theory. And Figure 1c confirms the importance of the compensations between Ekman and geostrophic cross-shore transport in the SSUC, with T_W being a small negative (seaward) residual between large onshore geostrophic and offshore Ekman flows.

A marked decrease in upwelling rate is manifest in Figure 1b for all CC simulations. In S_W, it is a bit more pronounced than the wind decrease (14% vs. 10%), that is, close to 2D Ekman expectation. Note though, that large compensations occur between less transport out of the control volume at the western boundary and more at the southern (which is due in large part to the stronger eastward component of the wind and thus stronger southward Ekman transport under CC). On the other hand, both simulations with stratification CC perturbations undergo significantly stronger IS_w reductions, by 24% and 26% for S_{W-SC} and S_{W-S} respectively. As expected, these reductions go hand in hand with diminished lateral fluxes out of the box at the western boundary but with a small mismatch due to the fact that the transport out of the box at the southern boundary increases slightly under CC. Significance tests (Student's t test) carried out on the mass balance terms (see Table S3 in Supporting Information S1) show that changes in T_S, T_{hbl} and ϵ are not significant at 80%, so we do not elaborate further.

Additional insight into T_W changes can be gained from Figure 1c. These changes are essentially determined by changes in geostrophic and Ekman flow while ϵ_{T_W} plays an insignificant role. Importantly, the geostrophic transport does not respond simply to wind intensity and also depends on stratification. The case with the lowest upwelling rate is S_{W-S} in which a complete cancellation occurs between Ekman and geostrophic flows. T_W is also strongly reduced (by 2/3 of its present-day value) when a horizontally homogeneous stratification CC

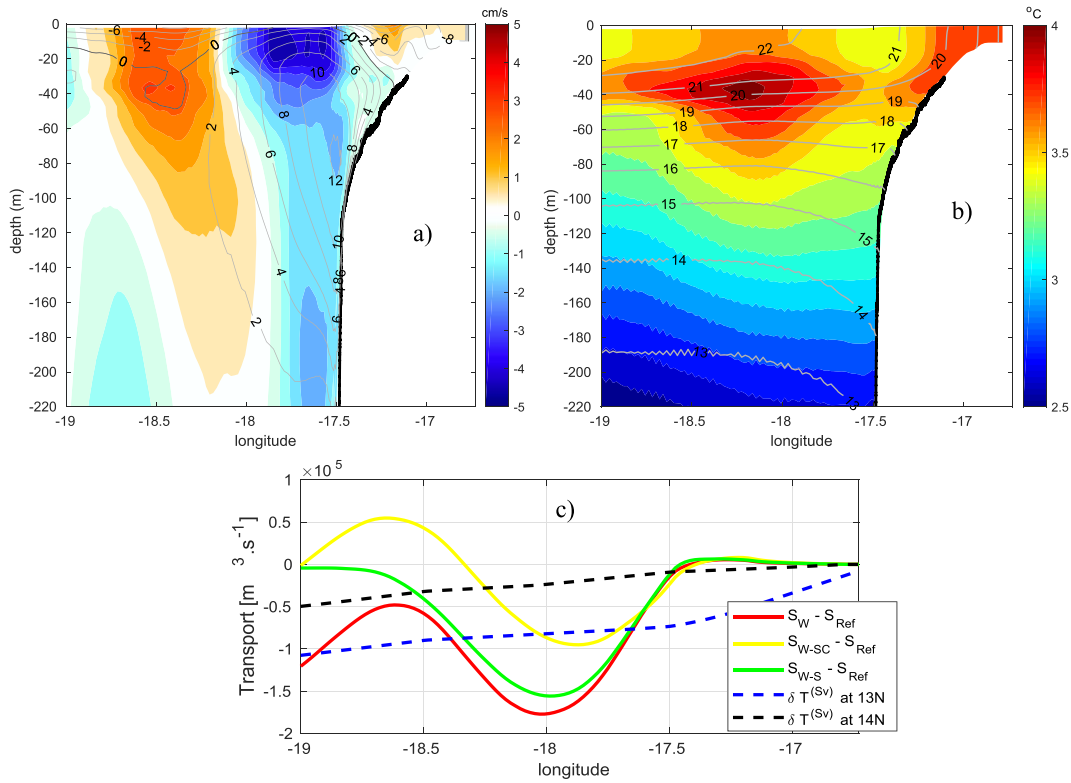

Figure 2. (a) Depth-longitude section of meridional velocity anomaly ((S_{W-S} -S_{Ref}, in m s^{-1}), color scale) along 14° N. S_{Ref} meridional velocity is indicated by gray contours (positive values indicate northward flow; the zero contour is indicated in bold gray). (b) Depth-longitude section of temperature anomaly (S_{W-S} -S_{Ref}, in °C, color scale). S_{Ref} temperature is marked by gray contours. (c) Depth-integrated meridional transport anomalies (with respect to S_{Ref}) along 14N for the three climate change simulations. Sverdrup cross-shore accumulated transport anomalies at latitudes 13°N and 14° N are also indicated. Vertical integration is performed from the surface to the 210 m depth (at which the poleward undercurrent is almost non-existent). The cross-shore accumulation of Sverdrup transport is performed from the shoreline ∼ 16.75°N to offshore.

perturbation is imposed (S_{W-SC}). Note that near zero T_W do not imply vanishing cross-shore velocities but rather an almost perfect cancellations between inflowing and outgoing surface flow at the western boundary. Large entries of water into the shelf still exist within 50 km south of Cap vert (14.8°N) as part of a quasi-standing anticyclonic circulation feature (not shown). Some subtleties in flow response to CC revealed in Figures 1b and 1c may be indirect consequences of how the dynamics of this nonlinear feature is affected. The response to enhanced upper ocean stratification in the form of reduced upwelling is presumably more generic (Di Lorenzo et al., 2005).

3.3. Changes in Meridional Circulation

Boundary currents have important implications on EBUS functioning because they carry the subsurface source waters for coastal upwelling. Meridional velocity changes are examined in the heart of the SSUC, at 14°N (Figure 2a). The model circulation (contours) is consistent with the state of knowledge for the area (Capet et al., 2017; Kounta et al., 2018; Ndoye et al., 2018; Roy, 1998) with an equatorward surface current over the inner and mid-shelf (i.e., the upwelling jet) and a poleward flowing counter-under-current over the outer shelf and slope. Nearshore, the equatorward coastal jet is projected to slow down slightly in S_W (Figure S4 in Supporting Information S1), in agreement with the upwelling reduction. Over the upper slope, a robust slowdown of the poleward undercurrent is projected, particularly in the surface layer (e.g., ∼−5 cm s^{-1} at 20 m depth). Similar results are found for S_{W-S} (Figure 2a) and S_{W-SC} (Figure S4 in Supporting Information S1).

In an attempt to establish a link between this poleward transport reduction and wind CC perturbation, we calculate the perturbations in vertically and cross-shore integrated meridional transport ($\delta T_y(x)$) for all simulations as well

as the perturbations expected from Sverdrup theory ($\delta T_y^{(Sv)}(x)$) (Sverdrup et al., 1942) (Figure 2c; see Text S3 in Supporting Information S1 for mathematical expressions). Vertical integration is performed from 210 m to the ML base (Kounta et al., 2018). Sverdrup balance should not be satisfied precisely and some caveats are worth mentioning. With the full barotropic vorticity balance in mind (Waldman & Giordani, 2023), discrepancies can arise from transient effects since our diagnostics are carried out over the upwelling season and the signature of wind-forced westward propagating Rossby waves remains present (in form of a trough at ∼ 18°W and a crest in transport at ∼ 18.7°W in Figure 2c). In fact, annual mean quantities exhibit reduced zonal oscillations (see Figure S5 in Supporting Information S1) and better agreement with Sverdrup theory. Nonlinearities (and numerical viscosity) can also contribute to cross-shore redistributions of meridional momentum as previously shown for the California current system (Marchesiello et al., 2003). Finally, wind stress curl CC perturbations vary rapidly with latitude in the SSUC such that Sverdrup transport perturbations $\delta T_y^{(Sv)}$ computed at 14°N or a bit to the north or south differ strongly (Figure 2c).

Beside these caveats, the substantial differences between the zonal profiles of δT_y for experiments S_{W-SC} and S_{W-S} (Figure 2c) call for caution. Both in seasonal and annual mean, the effect of the density CC perturbation on δT_y is present offshore of 18°W that Sverdrup theory is unable to explain. Pending more in-depth investigation, we note that the poleward boundary current is projected to weaken south of 15°N as winds change due to CC. Depending on the experiment the magnitude of the transport weakening from the coast to 18°W varies in the range 0.1–0.2 Sv, that is, 12%–24% of the transport in S_{Ref}. The latitudinal dependence of $\delta T_y^{(Sv)}$ implies that the zonal flow patterns should also be affected with more onshore transport where $\partial_y \delta T_y^{(Sv)} \propto \partial_y \delta(\nabla \times \tau) > 0$, that is, roughly between 14 and 18°N (Figure 1a). This may contribute to the coastal upwelling changes studied in the previous section (via flow (T_W) and pressure field adjustments at the shelf break).

3.4. Changes of the Thermal Structure

Temperature changes ($\delta\theta$) due to wind changes only (in S_W) are expectedly weak (<0.3°C, Figure S6a in Supporting Information S1) over the upper part of the water column (0–200 m). Nevertheless, temperature increases nearshore as expected from coastal upwelling reduction. Offshore $\delta\theta$ appear tightly related to meridional circulation changes, that is, the poleward flow increase with CC (Figure S4a in Supporting Information S1) leads to positive $\delta\theta$ (and conversely for poleward flow decrease). In contrast, notable warming are found in S_{W-S} nearshore (∼3.5°C) and offshore (up to ∼4°C; Figure 2b), consistently with the CMIP5 $\delta\theta$ (Figure S7 in Supporting Information S1). While meridional advection clearly drives $\delta\theta$ in S_W, this same effect resulting from circulation changes is of second order relative to the $\delta\theta$ resulting from large-scale temperature CC perturbations (Figure 2b and Figure S6b in Supporting Information S1 for S_{W-SC}). The induced changes in thermocline depth have a largest impact on subsurface temperature where the temperature vertical gradient is large. The temperature perturbations induce moderate stratification increases (∼10%) between 40 and 100 m depth (Figure S8 in Supporting Information S1).

The attenuation of temperature changes with increasing depth is a well understood feature of CC manifestation in the ocean (Stouffer, 2004). The attenuation toward the surface is more surprising (Figure 2b). This characteristic is also found in the CMIP5 temperature/density CC perturbations (see Figure S7 in Supporting Information S1). In our simulations, it could not have been directly inherited from CC perturbations imposed at the oceanic boundaries given the size of our domain and the importance of local processes in the determination of the near-surface thermohaline properties. An alternative explanation is that this slight attenuation of $\delta\theta$ toward the surface is a consequence of our heat flux CC perturbation protocol. Indeed, by imposing fixed CC perturbations for the restoring SST and for the net heat flux (see Text S1 in Supporting Information S1), model δSST becomes the adjustment variable to ensure compatibility with the dynamical changes and how they affect the heat budget (via advection and diffusion). To estimate the relevance of this thermodynamical explanation we have computed the magnitude of the SSUC-averaged restoring term for all our experiments. We find that it is 2 (S_{W-SC}) to 3 (S_{W-S}) W m^{-2} stronger when thermohaline CC perturbations are present (S_{W-S} and S_{W-SC}) than when it is not (S_{Ref} and S_W). Everything else remaining equal and given values of $\frac{dQ}{dSST}$ (∼30 W m^{-2} K^{-1}; see Text S2 in Supporting Information S1), these 2–3 W m^{-2} included into the net air-sea heat flux term translate into a SST increase of $0.07-0.1$°C. This corresponds to only 1/3-1/2 of the near-surface $\delta\theta$ attenuation. This and the fact that the subsurface $\delta\theta$ maximum is more pronounced in S_{W-S} than in S_{W-SC} suggest that other causes are involved.

Regional scale positive wind stress curl and Ekman suction a priori disqualify mean vertical advection as a simple way to locally propagate CC surface warming into the ocean interior (as found for the subtropical Canary system by Chang et al., 2023). Lateral transport of remotely subducted anthropogenic warming signal along subsurface central waters pathways (Zhang et al., 2003) may be important and help produce our original $\delta\theta$ vertical structure.

4. Discussion and Conclusions

4.1. Summary of the Results

Through dynamical downscaling of CMIP5 projections under the RCP8.5 scenario, we explored the physical manifestations of CC at the 2080–2100 horizon during the upwelling season (January–May) in the southern Senegal upwelling center (SSUC; 12.5-15°N). This is investigated by means of a high resolution regional ocean circulation model. In the context of the worst-case, high emission scenario (RCP8.5), our findings for this sector are that:

- A ∼10% reduction of upwelling favorable winds yields a ∼15% weakening of the coastal upwelling rate;
- Upper ocean temperature increases by 2.5−3.5°C with larger increases near ∼30−50 m depth so that stratification also increases by ∼10% in the upper thermocline;
- The CC-induced increase in near-surface stratification further contributes to the weakening of coastal upwelling (minus 25% when combining wind and stratification effects with little sensitivity to regional heterogeneities in CC stratification modifications, i.e., S_{W-SC} and S_{W-S} behave similarly);
- The spatial pattern of CC induced wind change leads to a reduction of the offshore wind stress curl, Ekman suction and poleward undercurrent (the WABC) through Sverdrup dynamics.

4.2. Tropicalization in the Tropics

An expected manifestation of CC is the tropicalization of mid-latitude marine ecosystems. Although located in the tropics, the typical temperatures and ecosystem functioning of the SSUC more closely resemble those of mid-latitude areas for much of the year (Arístegui et al., 2009; Rébert, 1983; Tall et al., 2021). During the monsoon season, tropical species are known to migrate into the system from the south (Corten et al., 2017), thereby producing what may be seen as a seasonal scale tropicalization. In the light of large-scale studies such as Sylla et al. (2019), long term trends in upwelling intensity seem modest and the risk of greater SSUC tropicalization appears limited. Making use of higher numerical resolution and state-of-the-art physical modeling, we project a more severe reduction in upwelling intensity both nearshore and offshore. This means a higher risk that the southern extremity of the West African upwelling system would move poleward. This may be mitigated somewhat by the fact that a future reduction in offshore upwelling goes hand in hand with a reduced northward slope transport of tropical water off the SSUC, hence a minor attenuation of the local ocean warming and of the passive displacement of tropical species toward the SSUC. But upper ocean temperature is nonetheless projected to increase by 2.5-3°C, likely larger than in recent high resolution global coupled models allowing ocean-atmosphere feedbacks (Chang et al., 2023) although a precise comparison would require further investigation. Even for smaller temperature increases, impacts on zooplankton community structure are plausible given that the dominant species (*Calanoides Carinatus*) appears negatively affected by temperatures above 23°C (Diouf, 1991; Wiafe et al., 2008). This link in the trophic chain would warrant appropriate monitoring.

4.3. Role of Pressure Adjustment to CC Perturbations

Compensation of offshore Ekman transport by onshore geostrophic currents is a major dynamical process, which needs to be taken into account to estimate coastal upwelling accurately (Colas et al., 2008; Jacox et al., 2018; Oerder et al., 2015), in particular in the SSUC (Ndoye et al., 2017). And CC induced geostrophic currents mitigating or amplifying coastal upwelling have been identified in some EBUS regions. In the Peruvian upwelling system (Oerder et al., 2015) found that the onshore geostrophic flow decreased under CC, compensating for the Ekman transport decrease and yielding an unchanged net upwelling during the peak upwelling season. In the California current system (Ding et al., 2021) found that CC changes in the onshore geostrophic transport were strongly season and latitude dependant.

In the SSUC this process also modulates projected changes in overall upwelling intensity which decreases more (14%) than Ekman transport (10%) in S_W in which everything but the wind remains unchanged. In S_{W-S} and S_{W-SC}

the effect is further amplified by stratification increase and upwelling reduction reaches −25%–30%. This stratification impact is qualitatively consistent with the one found by Di Lorenzo et al. (2005) in their study of the historical warming of the California Current system.

4.4. Perspectives

Downscaling state-of-the-art CMIP6 scenarios would be instructive given that their numerical resolutions tend to be higher and their biases weaker with respect to CMIP5. Carrying out Lagrangian experiments in the manner of Ndoye et al. (2017) would be informative on any change in water depth for upwelling source waters in the SSUC. Performing heat budgets for the different simulations would help clarify the processes involved in the surface and subsurface thermohaline changes due to CC. Last, our study will need to be complemented by regional simulations with a biogeochemical model to assess the degree to which essential variables (such as dissolved oxygen and nutrient concentration, primary production, …) are being impacted by CC. Such downscaling may help reduce the ESM biogeochemical biases and allow to investigate the regional trends (Echevin et al., 2020; Howard et al., 2020).

Data Availability Statement

The code can be freely downloaded via (Ndoye, 2024b). Model climatologies and scripts to reproduces the article's figures can be freely downloaded via (Ndoye, 2024a).

Acknowledgments
S.N. was supported by the Future Climate for Africa (FCFA)—AMMA 2050 innovative fund (SCUS-2050 project Grant M0220428/1), IRD and Université Amadou Mahtar MBOW. This work benefited from Agence nationale de la recherche fundings (SOLAB ANR-18-CE32- 0009). ROMS simulations were performed on the Irene skylake TGCC HPC under DARI projects A0110101140 and A0130101140. The authors thank Dr. Moussa Diakhate and Pr Amadou Thierno Gaye for the coordination of the SCUS-FCFA project marine part of the AMMA project, Dr. Adama Sylla and Dr. Lala Kounta for useful initial discussions.

References

Arístegui, J., Barton, E. D., Álvarez-Salgado, X. A., Santos, A. M. P., Figueiras, F. G., Kifani, S., et al. (2009). Sub-regional ecosystem variability in the canary current upwelling. *Progress in Oceanography*, *83*(1–4), 33–48. https://doi.org/10.1016/j.pocean.2009.07.031

Barnier, B., Siefried, L., & Marchesiello, P. (1995). Thermal forcing for a global ocean circulation model using a three-year climatology of ECMWF analyses. *Journal of Marine Systems*, *6*, 363–380.

Barton, E. D. (1998). Eastern boundary of the north Atlantic: Northwest Africa and Iberia. Coastal segment. In A. R. Robinson & K. H. Brink (Eds.), *The Sea: The global coastal ocean* (Vol. 11, pp. 633–657). Wiley.

Bograd, S. J., Jacox, M. G., Hazen, E. L., Lovecchio, E., Montes, I., Pozo Buil, M., et al. (2023). Climate change impacts on eastern boundary upwelling systems. *Annual Review of Marine Science*, *15*(1), 303–328. https://doi.org/10.1146/annurev-marine-032122-021945

Boyer, T., Locarnini, R. A., Baranova, O., Garcia, H. E., Mishonov, A. V., Paver, C., et al. (2018). The World Ocean Atlas 2018: Improvements and uses of climatological mean fields. *Agu fall meeting abstracts*, *2018*, OS13D–1506.

Capet, X., Estrade, P., Machu, E., Ndoye, S., Grelet, S., Lazar, A., et al. (2017). On the dynamics of the southern Senegal upwelling center: Observed variability from synoptt IC to super-inertial scales. *Journal of Physical Oceanography*, *47*(1), 155–180. https://doi.org/10.1175/jpo-d-15-0247.1

Capet, X., Marchesiello, P., & McWilliams, J. C. (2004). Upwelling response to coastal wind profiles. *Geophysical Research Letters*, *31*(13), L13311. https://doi.org/10.1029/2004gl020123

Capson, T. L., Machu, E., Boye, M., Schmidt, J. O., Thomas, Y., Capet, X., & Diouf, M. (2021). Expanding ocean observation and climate services to build resilience in West African fisheries. *One Earth*, *4*(8), 1062–1065. https://doi.org/10.1016/j.oneear.2021.07.010

Carton, J., & Giese, B. (2008). A reanalysis of ocean climate using Simple Ocean Data Assimilation (SODA). *Monthly Weather Review*, *136*(8), 2999–3017. https://doi.org/10.1175/2007mwr1978.1

Chabert, P., Capet, X., Echevin, V., Lazar, A., Hourdin, C., & Ndoye, S. (2023). Impact of synoptic wind intensification and relaxation on the dynamics and heat budget of the south Senegalese upwelling sector. *Journal of Physical Oceanography*, *53*(4), 1041–1067. https://doi.org/10.1175/JPO-D-22-0092.1

Chang, P., Xu, G., Kurian, J., Samll, R. J., Danabasoglu, G., Yeager, S., et al. (2023). Uncertain future of sustainable fisheries environment in eastern boundary upwelling zones under climate change. *Nature communications Earth Environ*, *4*(1), 19. https://doi.org/10.1038/s43247-023-00681-0

Colas, F., Capet, X., McWilliams, J. C., & Shchepetkin, A. (2008). 1997-98 El Nino off Peru: A numerical study. *Progress in Oceanography*, *79*(2–4), 138–155. https://doi.org/10.1016/j.pocean.2008.10.015

Corten, A., Braham, C.-B., & Sadegh, A. S. (2017). The development of a fishmeal industry in Mauritania and its impact on the regional stocks of Sardinella and other small Pelagics in northwest Africa. *Fisheries Research*, *186*, 328–336. https://doi.org/10.1016/j.fishres.2016.10.009

D'Agostino, R., Scambiati, A. L., Jungclaus, J., & Lionello, P. (2020). Poleward shift of northern subtropics in winter: Time of emergence of zonal versus regional signals. *Geophysical Research Letters*, *47*(19), e2020GL089325. https://doi.org/10.1029/2020gl089325

Debreu, L., Marchesiello, P., Penven, P., & Cambon, G. (2012). Two-way nesting in split-explicit ocean models: Algorithms, implementation and validation. *Ocean Modelling*, *49–50*, 1–21. https://doi.org/10.1016/j.ocemod.2012.03.003

Demarcq, H., & Faure, V. (2000). Coastal upwelling and associated retention indices derived from satellite SST. Application to octopus vulgaris recruitment. Ocean. *Acta*, *23*(4), 391–408. https://doi.org/10.1016/s0399-1784(00)01113-0

Di Lorenzo, E., Miller, A. J., Schneider, N., & McWilliams, J. C. (2005). The warming of the California current system: Dynamics and ecosystem implications. *Journal of Physical Oceanography*, *35*(3), 336–362. https://doi.org/10.1175/jpo-2690.1

Ding, H., Alexander, M. A., & Jacox, M. G. (2021). Role of geostrophic currents in future changes of coastal upwelling in the California current system. *Geophysical Research Letters*, *48*(3), e2020GL090768. https://doi.org/10.1029/2020GL090768

Diouf, P. (1991). Le zooplancton au sénégal. In *Pêcheries ouest africaines: variabilité, instabilité et changement. paris, cury p. et roy c.* (116, p. 103).

Echevin, V., Gévaudan, M., Espinoza-Morriberón, D., Tam, J., Aumont, O., Gutierrez, D., & Colas, F. (2020). Physical and biogeochemical impacts of RCP8.5 scenario in the Peru upwelling system. *Biogeosciences*, *17*(12), 3317–3341. https://doi.org/10.5194/bg-17-3317-2020

Echevin, V., Goubanova, K., Belmadani, A., & Dewitte, B. (2012). Sensitivity of the Humboldt current system to global warming: A downscaling experiment of the IPSL-CM4 model. *Climate Dynamics*, *38*(3–4), 761–774. https://doi.org/10.1007/s00382-011-1085-2

Enfield, D. B., & Allen, J. (1980). On the structure and dynamics of monthly mean sea level anomalies along the pacific coast of north and south America. *Journal of Physical Oceanography*, *10*(4), 557–578. https://doi.org/10.1175/1520-0485(1980)010<0557:otsado>2.0.co;2

Fall, S., Semazzi, F. H. M., Niyogi, D. D. S., Anyah, R. O., & Bowden, J. (2006). The spatiotemporal climate variability over Senegal and its relationship to global climate. *International Journal of Climatology*, *26*(14), 2057–2076. https://doi.org/10.1002/joc.1355

Garreaud, R., & Muñoz, R. (2005). The low-level jet off the West coast of subtropical South America: Structure and variability. *Monthly Weather Review*, *133*(8), 2203–2261. https://doi.org/10.1175/mwr2972.1

Hall, A., Cox, P., Huntingford, C., & Klein, S. (2019). Progressing emergent constraints on future climate change. *Nature Climate Change*, *9*(4), 269–278. https://doi.org/10.1038/s41558-019-0436-6

He, C., Wu, B., Zou, L., & Zhou, T. (2017). Responses of the summertime subtropical anticyclones to global warming. *Journal of Climate*, *30*(16), 6465–6479. https://doi.org/10.1175/jcli-d-16-0529.1

Howard, E. M., Frenzel, H., Kessouri, F., Renault, L., Bianchi, D., McWilliams, J. C., & Deutsch, C. (2020). Attributing causes of future climate change in the California current system with multimodel downscaling. *Global Biogeochemical Cycles*, *34*(11), e2020GB006646. https://doi.org/10.1029/2020GB006646

Hughes, P., & Barton, E. (1974). Stratification and water mass structure in the upwelling area off northwest Africa in April/May 1969. *Deep-Sea Research and Oceanographic Abstracts*, *21*(8), 611–628. https://doi.org/10.1016/0011-7471(74)90046-1

Jacox, M. G., Edwards, C. A., Hazen, E. L., & Bograd, S. J. (2018). Coastal upwelling revisited: Ekman, Bakun, and improved upwelling indices for the U.S. West Coast. *Journal of Geophysical Research: Oceans*, *123*(10), 7332–7350. https://doi.org/10.1029/2018JC014187

Klenz, T., Dengler, M., & Brandt, P. (2018). Seasonal variability of the Mauritania current and hydrography at 18°n. *Journal of Geophysical Research: Oceans*, *123*(11), 8122–8137. https://doi.org/10.1029/2018JC014264

Kounta, L., Capet, X., Jouanno, J., Kolodziejczyk, N., Sow, B., & Gaye, A. T. (2018). A model perspective on the dynamics of the shadow zone of the eastern tropical north Atlantic. Part 1: The poleward slope currents along West Africa. *Ocean Science Discussions*, 1–40. https://doi.org/10.5194/os-2018-16

Lee, T., Waliser, D. E., Li, J.-L. F., Landerer, F. W., & Gierach, M. M. (2013). Evaluation of CMIP3 and CMIP5 wind stress climatology using satellite measurements and atmospheric reanalysis products. *Journal of Climate*, *26*(16), 5810–5826. https://doi.org/10.1175/JCLI-D-12-00591.1

Lellouche, J.-M., Greiner, E., Le Galloudec, O., Garric, G., Regnier, C., Drevillon, M., et al. (2018). Recent updates to the Copernicus marine service global ocean monitoring and forecasting real-time 1/12∘ high-resolution system. *Ocean Science*, *14*(5), 1093–1126. https://doi.org/10.5194/os-14-1093-2018

Machu, E., Goubanova, K., Le Vu, B., Gutknecht, E., & Garçon, V. (2015). Downscaling biogeochemistry in the Benguela eastern boundary current. *Ocean Modelling*, *90*, 57–71. https://doi.org/10.1016/j.ocemod.2015.01.003

Marchesiello, P., Capet, X., Menkes, C., & Kennan, S. C. (2011). Submesoscale turbulence in tropical instability waves. *Ocean Modelling*, *39*(1–2), 31–46. https://doi.org/10.1016/j.ocemod.2011.04.011

Marchesiello, P., McWilliams, J. C., & Shchepetkin, A. (2003). Equilibrium structure and dynamics of the California current system. *Journal of Physical Oceanography*, *33*(4), 753–783. https://doi.org/10.1175/1520-0485(2003)33<753:esadot>2.0.co;2

Mittelstaedt, E. (1991). The ocean boundary along the northwest African coast: Circulation and oceanographic properties at the sea surface. *Progress in Oceanography*, *26*(4), 307–355. https://doi.org/10.1016/0079-6611(91)90011-a

Ndoye, S. (2024a). Datasets and scripts to reproduce figures from the paper entitled "Impact of climate change on the dynamics of the Southern Senegal Upwelling Center". *Zenodo*. https://doi.org/10.5281/zenodo.10664488

Ndoye, S. (2024b). ROMS model code. *Zenodo*. https://doi.org/10.5281/zenodo.10664817

Ndoye, S., Capet, X., Estrade, P., Machu, E., Kounta, L., Sow, B., & Gaye, A. T. (2018). A numerical modeling study of the southern Senegal upwelling shelf: Circulation and upwelling source waters. *African Journal of Environmental Science and Technology*, *12*(12), 487–500. https://doi.org/10.5897/AJEST2018.2572

Ndoye, S., Capet, X., Estrade, P., Sow, B., Dagorne, D., Lazar, A., et al. (2014). SST patterns and dynamics of the southern Senegal-Gambia upwelling center. *Journal of Geophysical Research*, *119*(12), 8315–8335. https://doi.org/10.1002/2014jc010242

Ndoye, S., Capet, X., Estrade, P., Sow, B., Machu, E., Brochier, T., et al. (2017). Dynamics of a "low-enrichment high-retention" upwelling center over the southern Senegal shelf. *Geophysical Research Letters*, *44*(10), 5034–5043. https://doi.org/10.1002/2017GL072789

Oerder, V., Colas, F., Echevin, V., Codron, F., Tam, J., & Belmadani, A. (2015). Peru-Chile upwelling dynamics under climate change. *Journal of Geophysical Research: Oceans*, *120*(2), 1152–1172. https://doi.org/10.1002/2014JC010299

Particola, C., & Chang, P. (2017). Structure and dynamics of the benguela low-level coastal jet. *Climate Dynamics*, *49*(7–8), 2765–2788. https://doi.org/10.1007/s00382-016-3479-7

Pozo Buil, M., Fiechter, J., Jacox, M. G., Bograd, S. J., & Alexander, M. A. (2023). Evaluation of different bias correction methods for dynamical downscaled future projections of the California current upwelling system. *Earth and Space Science*, *10*(12), e2023EA003121. https://doi.org/10.1029/2023EA003121

Praveen Kumar, B., Vialard, J., Lengaigne, M., Murty, V., McPhaden, M., Cronin, M., et al. (2013). Tropflux wind stresses over the tropical oceans: Evaluation and comparison with other products. *Climate Dynamics*, *40*(7–8), 2049–2071. https://doi.org/10.1007/s00382-012-1455-4

Rébert, J. (1983). Hydrologie et dynamique des eaux du plateau continental sénégalais. *Doc. Scient. Centre Rech.Océanog.Dakar-Thiaroye*, *67*, 14p.

Renault, L., Hall, A., & McWilliams, J. C. (2015). Orographic shaping of US West Coast wind profiles during the upwelling season. *Climate Dynamics*, *46*(1–2), 273–289. https://doi.org/10.1007/s00382-015-2583-4

Ribes, A., Boé, J., Qasmi, S., Dubuisson, B., Douville, H., & Terray, L. (2022). An updated assessment of past and future warming over France based on a regional observational constraint. *Earth System Dynamics*, *13*(4), 1397–1415. https://doi.org/10.5194/esd-13-1397-2022

Roy, C. (1998). An upwelling-induced retention area off Senegal: A mechanism to link upwelling and retention processes. *South African Journal of Marine Science*, *19*(1), 89–98. https://doi.org/10.2989/025776198784126881

Rykaczewski, R. R., Dunne, J. P., Sydeman, W. J., García-Reyes, M., Black, B. A., & Bograd, S. J. (2015). Poleward displacement of coastal upwelling-favorable winds in the ocean's eastern boundary currents through the 21st century. *Geophysical Research Letters*, *42*(15), 6424–6431. https://doi.org/10.1002/2015gl064694

Shchepetkin, A., & McWilliams, J. C. (2005). The regional oceanic modeling system: A split-explicit, free-surface, topography-following-coordinate ocean model. *Ocean Modelling*, *9*(4), 347–404. https://doi.org/10.1016/j.ocemod.2004.08.002

Small, R. J., Curchitser, E., Hedstrom, K., Kauffman, B., & Large, W. G. (2015). The benguela upwelling system: Quantifying the sensitivity to resolution and coastal wind representation in a global climate model. *Journal of Climate*, *28*(23), 9409–9432. https://doi.org/10.1175/JCLI-D-15-0192.1

Stouffer, R. J. (2004). Time scales of climate response. *Journal of Climate*, *17*(1), 209–217. https://doi.org/10.1175/1520-0442(2004)017<0209:tsocr>2.0.co;2

Sverdrup, H. U., Johnson, M. W., & Fleming, R. H. (1942). *The oceans: Their physics, chemistry, and general biology*. Prentice Hall.1087

Sylla, A., Mignot, J., Capet, X., & Gaye, A. T. (2019). Weakening of the Senegalo–Mauritanian upwelling system under climate change. *Climate Dynamics*, *53*(7), 4447–4473. https://doi.org/10.1007/s00382-019-04797-y

Tall, A. W., Machu, E., Echevin, V., Capet, X., Pietri, A., Corréa, K., et al. (2021). Variability of dissolved oxygen in the bottom layer of the southern Senegalese shelf. *Journal of Geophysical Research: Oceans*, *126*(5), e2020JC016854. https://doi.org/10.1029/2020JC016854

Vázquez, R., Parras-Berrocal, I., Koseki, S., Cabos, W., Sein, D., & Izquierdo, A. (2023). Seasonality of coastal upwelling trends in the Mauritania-senegalese region under RCP8.5 climate change scenario. *Science of The Total Environment*, *898*, 166391. https://doi.org/10.1016/j.scitotenv.2023.166391

Waldman, R., & Giordani, H. (2023). Ocean barotropic vorticity balances: Theory and application to numerical models. *Journal of Advances in Modeling Earth Systems*, *15*(4), e2022MS003276. https://doi.org/10.1029/2022ms003276

Wang, D.-P., & Jordi, A. (2011). Surface frontogenesis and thermohaline intrusion in a shelfbreak front. *Ocean Modelling*, *38*(1–2), 161–170. https://doi.org/10.1016/j.ocemod.2011.02.012

Wiafe, G., Yaqub, H. B., Mensah, M. A., & Frid, C. L. J. (2008). Impact of climate change on long-term zooplankton biomass in the upwelling region of the Gulf of Guinea. *ICES Journal of Marine Science*, *65*(3), 318–324. https://doi.org/10.1093/icesjms/fsn042

Winant, C., Dorman, D., Friehe, C., & Beardsley, R. (1988). The marine layer off northern California: An example of supercritical channel flow. *Journal of the Atmospheric Sciences*, *45*(23), 3588–3605. https://doi.org/10.1175/1520-0469(1988)045<3588:tmlonc>2.0.co;2

Worley, S. J., Woodruff, S., Reynolds, R., Lubker, S., & Lott, N. (2005). Icoads release 2.1 data and products. *International Journal of Climatology*, *25*(7), 823–842. https://doi.org/10.1002/joc.1166

Zhang, D., McPhaden, M. J., & Johns, W. E. (2003). Observational evidence for flow between the subtropical and tropical Atlantic: The Atlantic subtropical cells. *Journal of Physical Oceanography*, *33*(8), 1783–1797. https://doi.org/10.1175/2408.1